Organic Electronics 107 (2022) 106552

Contents lists available at ScienceDirect

Organic Electronics

journal homepage: www.elsevier.com/locate/orgel

Improving the efficiency and stability of in-air fabricated perovskite solar cells using the mixed antisolvent of methyl acetate and chloroform

Martin C. Eze [a,b], Hyginus U. Eze [b], Godwin N. Ugwuanyi [a], Mohammad Alnajideen [a], Abdulhamid Atia [a], Samuel C. Olisa [b], Victoria G. Rocha [a], Gao Min [a,*]

[a] School of Engineering, Cardiff University, Cardiff, CF 24 3AA, United Kingdom
[b] Department of Electronic Engineering, University of Nigeria, Nsukka, 410001, Enugu, Nigeria

ARTICLE INFO

Keywords:
Antisolvents
Dipole moment
Perovskite solar cells
Power conversion efficiency
Solar cell stability

ABSTRACT

Antisolvents play a significant role in obtaining high-quality perovskite films during the fabrication process. This paper reports a novel mixture of two antisolvents (methyl acetate and chloroform) that proves effective for fabricating high-quality perovskite films in a high humidity ambient. The results show that the use of methyl acetate alone as the antisolvent enables the fabrication of dense perovskite films ($MAPbI_3$) in a high humidity ambient, but with a rough surface, while mixing methyl acetate with an appropriate amount of chloroform produces not only dense perovskite films but also smooth surfaces. As a result, the power conversion efficiency (PCE) is increased from 17.1% of the devices treated with methyl acetate alone to 18.6% of the devices treated with the mixed antisolvent of methyl acetate (70%) and chloroform (30%). The stability of the devices was also improved significantly for the devices treated with the mixed antisolvent of methyl acetate (85%) and chloroform (15%), which exhibit a slow degradation of 7% in PCE after 552 h of storage, compared to 22% for the devices treated with methyl acetate alone.

1. Introduction

The high absorption coefficient, exceptional carrier mobility, high dielectric constant, tuneable bandgap, materials abundance and low fabrication cost have made Perovskite Solar Cells (PSCs) one of the most promising photovoltaic technologies [1–6]. These exceptional properties have led to considerable research activities in PSCs, which resulted in Power Conversion Efficiency (PCE) enhancement from 3.8% in 2009 [7] to 24.8% in 2020 [8] and 25.2% in 2021 [9]. Despite the high PCE achieved so far, PSCs have suffered from poor stability, which limits their commercialisation [10–18]. It has been extensively reported that perovskite materials, perovskite layer deposition environment and process are the major cause of instability in PSCs [19,20].

Antisolvents play a significant role in improving the PCE and stability of PSCs. The effectiveness of an antisolvent depends on its vapour pressure, water solubility and dipole moment at processing temperature [21]. Table 1 shows the relevant physical properties of frequently used antisolvents. The high water solubility of methyl acetate and ethyl acetate has proven effective in protecting $MAPbI_3$/DMSO adduct from interacting with moistures and water vapour during spin-coating of the perovskite films, particularly in high humidity environments [21,22]. Their high vapour pressure and low boiling point accelerate the evaporation of DMF and water vapour around the films [21]. However, these antisolvents have dipole moments comparable to that of DMSO, which can fast extract DMSO from the perovskite solution and result in less DMSO in the $MAPbI_3$/DMSO adduct. This could lead to a fast nucleation process and poor film morphology [23,24]. Additionally, antisolvents with high dipole moments reduce the proportion of methylammonium iodide (MAI) in the perovskite solution by extracting MAI from the solution during treatment, leading to low grain compactness [5,25–27], reduction in the film thickness and introduction of lead (IV) iodide at the film surface [28–30]. On the other hand, the antisolvents such as chloroform and toluene have low dipole moments relative to DMSO, therefore, they cannot extract DMSO quickly from perovskite solution, leaving excess DMSO in $MAPbI_3$/DMSO adduct. This can result in significant rewetting, a slow nucleation process and consequently poor film morphology and low grain compactness, especially at high humidity [23,24]. This study demonstrates that the control of stoichiometry of $MAPbI_3$/DMSO adduct is vital to ensure the quality of the perovskite films, which can be achieved by adjusting the dipole moment (polarity)

* Corresponding author.
E-mail address: min@cardiff.ac.uk (G. Min).

https://doi.org/10.1016/j.orgel.2022.106552
Received 16 March 2022; Received in revised form 9 May 2022; Accepted 11 May 2022
Available online 16 May 2022

Table 1
The relevant physical properties of commonly used antisolvents [31,32].

Antisolvent	Vapour pressure (mmHg) at 23 °C	Water solubility (%) at 23 °C	Boiling point (°C)	Dipole moment (D)
Chlorobenzene	9	0.05	131.00	1.55
Chloroform	160	0.50	61.15	1.04
Methyl acetate	173	25.00	56.90	1.71
Ethyl acetate	73	10.00	77.22	1.78
Diethyl ether	440	8.00	34.44	1.28
Propyl acetate	25	2.00	101.67	1.86
Butyl acetate	10	1.00	125.56	1.87
Toluene	21	0.07	110.00	0.38
Trifluorotoluene	39	0.10	103.46	2.86
2-Butanol	12	16.00	99.44	1.62
Diisopropyl ether	119	0.20	69.00	1.30

of the antisolvents [24]. Ideally, a suitable antisolvent should exhibit all preferred properties for a given fabrication environment. In practice, it is very difficult to find a single antisolvent that meets all criteria because there are several properties to be considered as shown in Table 1. Consequently, mixing two or more antisolvents to obtain the preferred properties has been employed as a possible approach [23].

A convenient method to adjust the dipole moment of antisolvents is by mixing two antisolvents of different dipole moments [23]. This approach has been applied to the fabrication of PSCs to achieve improved performances [33–36]. The first study on the effect of antisolvent mixing on PSC performance was conducted by Wang et al. in 2017. They demonstrated that the PCE of 17.8% was obtained for devices treated with a mixture of chlorobenzene and isopropanol compared to 16.1% for devices treated with chlorobenzene alone [33]. Yu et al. reported that the devices treated using the mixed chloroform and n-hexane exhibited a PCE of 17.1% compared to 15.8% for the devices treated with either chloroform or n-hexane [37]. In 2018, Chen et al. reported improved performance for the devices treated with a mixture of 2-butanol (*Sec*-butyl alcohol) and chlorobenzene or a mixture of 2-butanol and dimethyl ether antisolvents [23]. Since 2018, several other mixtures have been reported to show improved performance, including toluene and chlorobenzene [34], dimethyl and dichlorobenzene [34], and petroleum ether and ethyl acetate [35]. Although these studies contributed immensely to the development of antisolvent mixing techniques for PSC fabrication, they were performed in a glovebox of exceptionally low humidity (0.1 ppm–1.0 ppm or 0.00001%–0.0001%). Very recently, Jung et al. reported a strategy of combining mixed cations and mixed antisolvent treatment to fabricate PSCs in ambient air of relative humidity >40% and obtained improved stability and PCE of 20.55% using dibutyl ether and diethyl ether antisolvents [38]. Our work here focused on the effect of the mixed antisolvents for fabrication in ambient air at higher humidity range (50–55%). The objective of this paper is to investigate the influence of mixing methyl acetate with chloroform on the efficiency and stability of PSCs fabricated in the air at high humidity. The methyl acetate was chosen as the base antisolvent for this study because it has high vapour pressure and high-water solubility, which are suitable for high humidity fabrication. The chloroform was chosen to optimise the dipole moment of the resultant antisolvent mixture because of its relatively low dipole moment. The development of simple and effective mixed antisolvent process is crucial to low-cost and air-fabrication routes for preparing PSCs with enhanced efficiency and stability. This study aims to identify the most suitable mixture of methyl acetate and chloroform antisolvents for PSC fabrication in high humidity air.

2. Materials and methods

2.1. Materials

Fluorine-doped tin oxide (FTO, TEC-15, 15mm × 20 mm) glasses were purchased from Pingdingshan Mingshuo Technology Co. Ltd. The 2,2′,7,7′-Tetrakis (N, N -di-p-methoxyphenylamino)-9,9′-

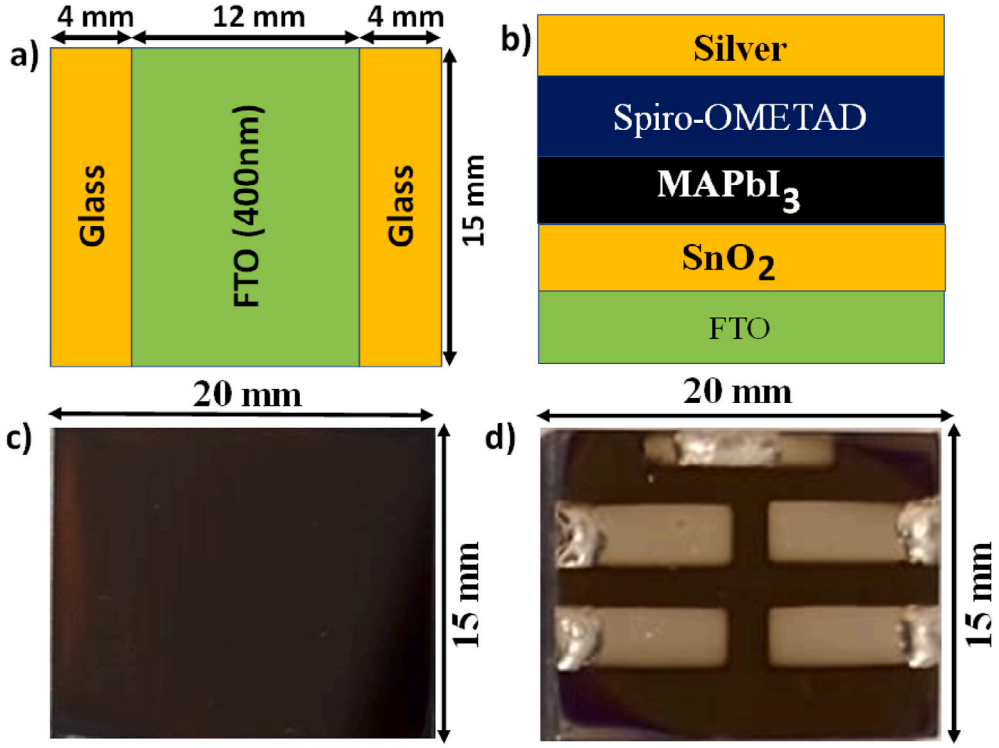

Fig. 1. (a) Dimensions of FTO glasses used in this work, (b) The structure of the perovskite solar cell, (c) The photograph of the perovskite film on FTO/SnO_2 substrate, and (d) The photograph of the silver electrodes on the fabricated device.

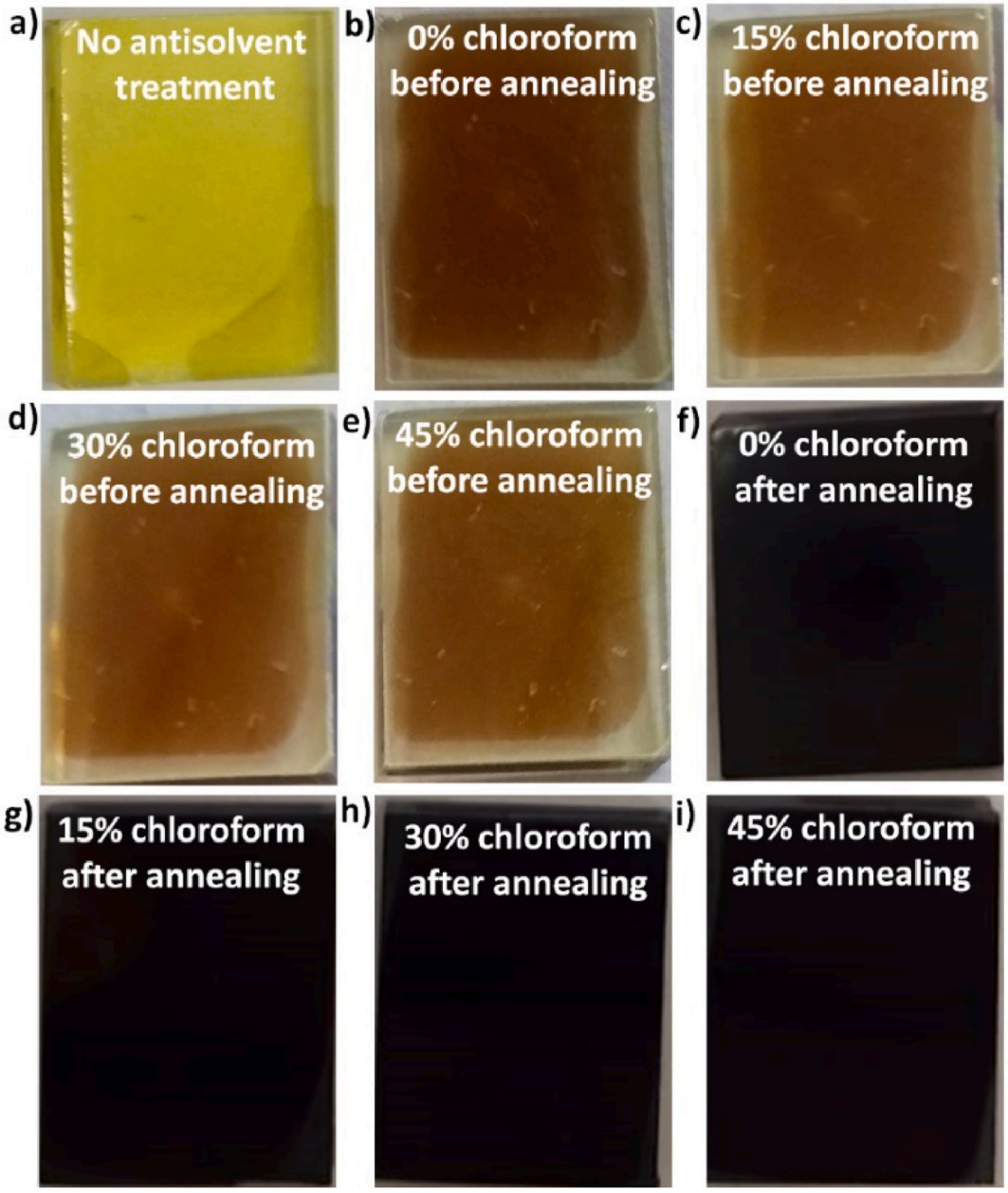

Fig. 2. Images of $MAPbI_3$ films treated with methyl acetate only and treated using the mixture of methyl acetate with chloroform before and after annealing. The films were deposited at 4000 rpm for 30 s and annealed at 110 °C for 15 min under 50–55% RH.

spirobifluorene (Spiro-OMETAD, 99.8%) was bought from Borun New Materials. Lead (II) iodide (PbI_2, 99.999%), lithium bis(trifluoromethylsulfonyl)imide (Li-TFSI, 98%), dimethyl sulfoxide (DMSO, 99.8%) and methyl acetate (MA, 99%) were bought from Alfa Aesar. Tris (2-(1H-pyrazol-1-yl)-a4-tert-butylpyridine) cobalt (III) tris(bis(trifluoromethylsulfonyl)imide) (FK209, 98%), Methylammonium iodide (MAI, 99%), tin (II) chloride dihydrate ($SnCl_2.2H_2O$, 99.995%) and 4-tert-Butylpyridine (TBP, 96%) were procured from Sigma Aldrich. Chlorobenzene (CB, 99.6%) and dimethylformamide (DMF, 99.8%) were obtained from Across Organics while acetonitrile (99.8%), chloroform, isopropanol, ethanol, and acetone were sourced from fisher scientific. Silver (Ag) target (99.99%, 2-inch diameter × 0.125-inch thick) was obtained from Kurt J. Lesker Company Ltd while a 0.45 μm hydrophilic nylon filter was procured from Ossila LTD.

2.2. Precursor solution preparation

$MAPbI_3$ solution was prepared by dissolving 722 mg of lead iodide (PbI_2) and 240 mg of methylammonium iodide (MAI) in 1 ml of a solvent mixture containing 200 μl of dimethyl sulfoxide (DMSO) and 800 μl of dimethylformamide (DMF). The solution was stirred at 300 rpm and 50 °C for 11 min before being filtered using a 0.45 μm syringe filter. Tin (IV) oxide precursor solution was prepared by dissolving 15 mg of tin (II) chloride dihydrate ($SnCl_2.2H_2O$) in 1 ml of ethanol and the solution was stirred at 300 RPM and 50 °C for 4 h before being filtered using a 0.45 μm syringe filter. The hole transport layer (HTL) solution was prepared by dissolving 90 mg of 2,2′,7,7′-Tetrakis(N, N -di-p -methoxyphenylamino)-9,9′- spirobifluorene (Spiro-OMeTAD) in 1 ml of chlorobenzene and then added with 38 μl of tris(2-(1H-pyrazol-1-yl)-4-tert-butylpyridine) cobalt(III) tri[bis(trifluoromethane)sulfonimide] (FK209) solution (300 gm/ml in acetonitrile), 36 μl of 4-tert-

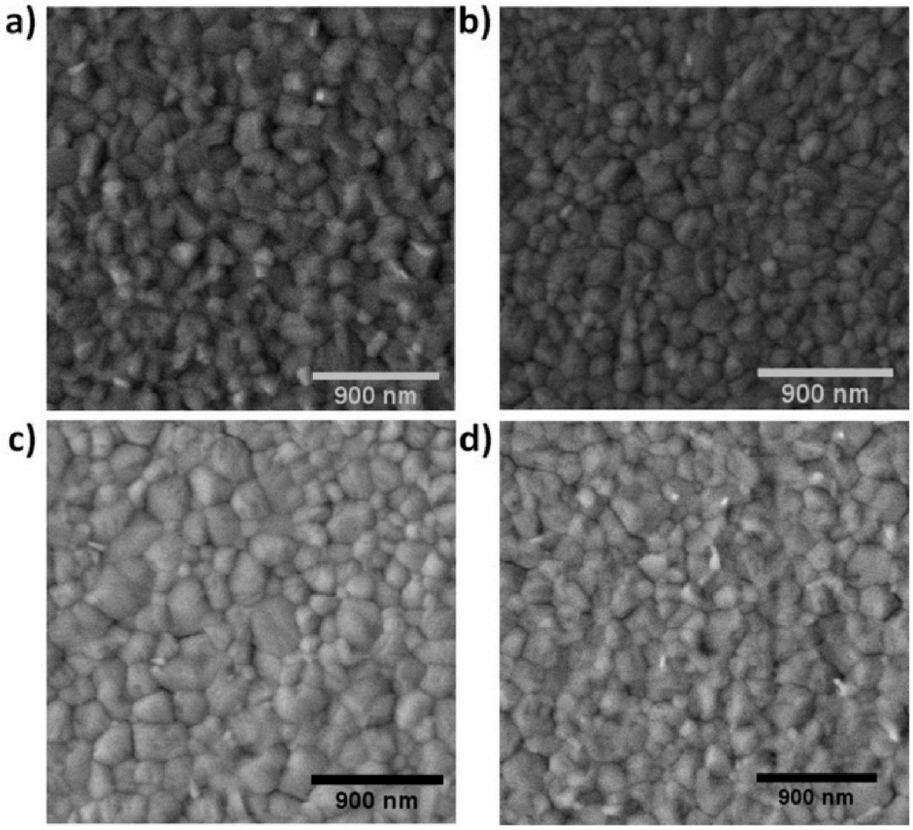

Fig. 3. SEM images of $MAPbI_3$ films treated with methyl acetate mixed with (a) 0% chloroform (b) 15% chloroform (c) 30% chloroform and (d) 45% chloroform. The films were deposited at 4000 rpm for 30 s and annealed at 110 °C for 15 min under 50–55% RH.

butylpyridine (BTP) and 22 μl of Lithium bis(trifluoromethanesulfonyl) imide (Li-TFSI) solution (520 mg/ml in acetonitrile). The solution was stirred at 30 °C and 300 rpm for 30 min.

2.3. Device fabrication

Hellmanex (III) solution was applied to thoroughly clean FTO glasses (20 mm × 15 mm) before the substrates were rinsed three times with deionized water. Then, the FTO glasses were successively cleaned in an ultrasonic bath at 50 °C for 10 min using deionized water, acetone, and isopropanol. Afterwards, the FTO glasses were dried using nitrogen gas and then, treated in the ultraviolet (UV)-ozone cleaner for 10 min. SnO_2 layers (electron transport layers, ETL) were prepared by spin coating 90 μl of $SnCl_2.2H_2O$ solution on FTO glasses at 4000 rpm for 30 s and the films were annealed at 180 °C for 60 min. The FTO glasses with the SnO_2 layers were treated for 10 min in a UV-Ozone cleaner. $MAPbI_3$ layers (perovskite layers) were prepared by spin-coating 90 μl of perovskite precursor on SnO_2 layers at 4000 rpm for 30 s. The films were then treated with 150 μl of antisolvents for 15 s, which contain methyl acetate mixed with 0%, 15%, 30% and 45% of chloroform, respectively. Dark $MAPbI_3$ films were obtained after annealing the films for 15 min at 110 °C. To ensure excellent film qualities, the $MAPbI_3$ films were deposited using the procedures reported in Ref 6. Subsequently, the Spiro-OMETAD layers were prepared by spin-coating 90 μl of Spiro-OMETAD solution on the $MAPbI_3$ layers at 4000 rpm for 30 s. Up to this point, all the films were prepared in the air at a relative humidity of 50–55%. Finally, the top electrode of 0.15 cm^2 was deposited on HTL using Ag by magnetron sputtering. The sputtering chamber was evacuated to 10 μTorr and refilled with argon gas before the Ag films deposition. The sputtering condition was set at 1.0 W, 15.0 standard cubic centimetres per minute (sccm), 5.0 mTorr and substrate temperature of 20 °C for 60 min.

2.4. Characterisation

The chemical composition of the films was characterised using an X-ray Diffractometer (XRD, Siemens D5000). Ultraviolet–Visible Spectrophotometer (UV-VIS, Hitachi U-1900) was used to study the optical properties of films. The perovskite film surface morphology was examined using an Atomic Force Microscope (AFM, dimension 3100) and Field emission Scanning Electron Microscope (FE-SEM, Carl Zeiss 1540XB system). A solar simulator (Oriel LCS-100, Class ABB) in conjunction with an AUTOLAB (Metrohm, PGSTAT302 N) was used for J-V measurement at standard test conditions (100 mW/cm^2, AM1.5G and 25 °C). The AUTOLAB equipped with a FRA32 M module was used for impedance spectroscopy measurement (IS) at 1.0 V and 100 mW/cm^2 illumination. The chemical capacitance of the devices was extracted from the IS data using Zsimdemo 3.2 software. A mask was placed above the PSC to ensure that the photocurrent is generated from a well-defined active area of the PSC.

3. Results and discussion

3.1. Properties of $MAPbI_3$ films

Fig. 1(a) and (b) present the layout of the FTO glass and the structure of fabricated devices (FTO/SnO_2/$MAPbI_3$/Spiro-OMETAD/Ag), respectively. Fig. 1(c) shows the fabricated perovskite film and Fig. 1(d) is a photograph of the complete device.

Fig. 2(a) shows the image of $MAPbI_3$ film before the application of antisolvent and annealing. Fig. 2(b)–2(e) show the image of $MAPbI_3$ films after the antisolvent treatment before annealing. The images show that the colour of the unannealed films becomes less dark as the proportion of chloroform increases from 0% to 45%. This suggests that films treated with only methyl acetate tend to form the perovskite phase (dark

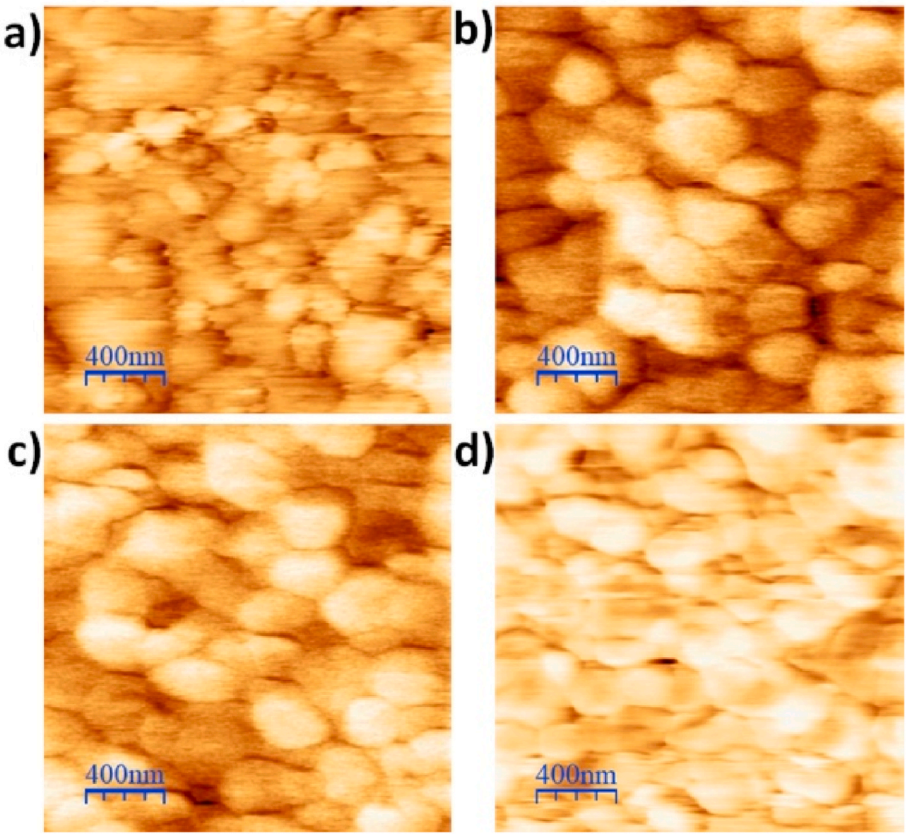

Fig. 4. AFM images of $MAPbI_3$ films treated with methyl acetate mixed with (a) 0% chloroform (b) 15% chloroform (c) 30% chloroform and (d) 45% chloroform. The films were deposited at 4000 rpm for 30 s and annealed at 110 °C for 15 min under 50–55% RH.

brown) directly because more DMSO was removed from the $MAPbI_3$/DMSO. When methyl acetate is mixed with chloroform, the rate of DMSO removal was reduced, leading to the formation of an intermediate perovskite phase of $MAPbI_3$/DMSO, which becomes more transparent [39]. Fig. 2(f)–2(i) present the images of the $MAPbI_3$ films after anti-solvent treatment and annealing. All the images appear dark, suggesting that they have reasonably good qualities of light absorption [22].

Fig. 3(a)–3(d) show the surface morphology of the $MAPbI_3$ films examined using FE-SEM for different percentages of chloroform in a mixed antisolvent of methyl acetate and chloroform. The SEM images show that all the films have reasonable crystallinity, morphology, and compactness. Furthermore, a detailed inspection shows that the film treated using the mixed antisolvent with 15% chloroform is smoother than that without chloroform. This can be attributed to a decrease in the dipole moment by mixing methyl acetate with chloroform, leading to a reduced rate of DMSO removal from perovskite precursor solution and producing the optimum $MAPbI_3$/DMSO adduct. As the chloroform proportion rose from 15% to 30%, the grain size is further increased. This is because the dipole moment of the mixed antisolvents was further reduced, leaving slightly more DMSO in the $MAPbI_3$/DMSO adduct. This slowed slightly the speed of the nucleation process and resulted in larger crystals, which are beneficial to improving the power conversion efficiency. However, the slow nucleation process in the $MAPbI_3$/DMSO adduct with excess DMSO may result in pinholes and defects between larger grains, which open pathways for moisture penetration and degradation in the stability. When the chloroform percentage was increased from 30% to 45%, the grain size and surface smoothness were degraded. This is because the dipole moment in the mixed antisolvents was further reduced, leading to drift from the optimum $MAPbI_3$/DMSO adduct due to excess DMSO and consequently a degradation in the film quality [23,24,40]. It can be estimated from SEM images that the average grain size is approximately 170 nm, 200 nm, 230 nm and 190 nm for films treated with methyl acetate mixed with 0%, 15%, 30% and 45% chloroform, respectively. These results show clearly that the perovskite films treated using a mixed antisolvent with the chloroform percentage between 15% and 30% appear to produce the best quality in terms of surface smoothness, grain size and compactness as shown in Fig. 3(b) and (c).

The morphology of the fabricated $MAPbI_3$ films was also examined using AFM and the results are shown in Fig. 4(a)–4(d) for the films treated using the methyl acetate mixed with 0%, 15%, 30% and 45% of chloroform, respectively. The AFM images indicate that the films exhibit good morphology of typical perovskite films for all films. However, the films treated with methyl acetate mixed 15% and 30% of chloroform appear to show better quality in terms of surface smoothness and grain size compared to the films treated with methyl acetate only or methyl acetate with mixed with 45% of chloroform. AFM image analysis using WSxM software confirms this observation. As shown in Fig. 5(a), the Root-Mean-Square (RMS) roughness is reduced significantly in the films treated using the mixed antisolvent with 15% and 30% chloroform. The RMS roughness for the films treated with methyl acetate mixed with 0%, 15%, 30% and 45% of chloroform are 25.60 ± 1.78 nm, 14.78 ± 1.67 nm, 13.53 ± 0.82 nm and 22.86 ± 2.11 nm, respectively. The improvement in the film smoothness is likely related to a decrease in the dipole moment of the mixed antisolvent as shown in Fig. 5(b), which was calculated using the method reported [41–44]. The net dipole moment for mixed antisolvent containing methyl acetate mixed with 0%, 15%, 30% and 45% of chloroform is estimated to be 1.706 D, 1.6061 D, 1.5062 D and 1.4063 D, respectively.

Fig. 5(c) and (d) show the XRD data of the FTO/$MAPbI_3$ films taken at 0 h and after 384 h of storage, respectively. The results obtained at 0 h show that $MAPbI_3$ peaks occurred at $2\theta = 14.1°$, 28.4° and 31.8° while the FTO peaks appeared at 37.9° and 26.6°, regardless of the addition of chloroform or not. These peaks agree with the peaks reported elsewhere

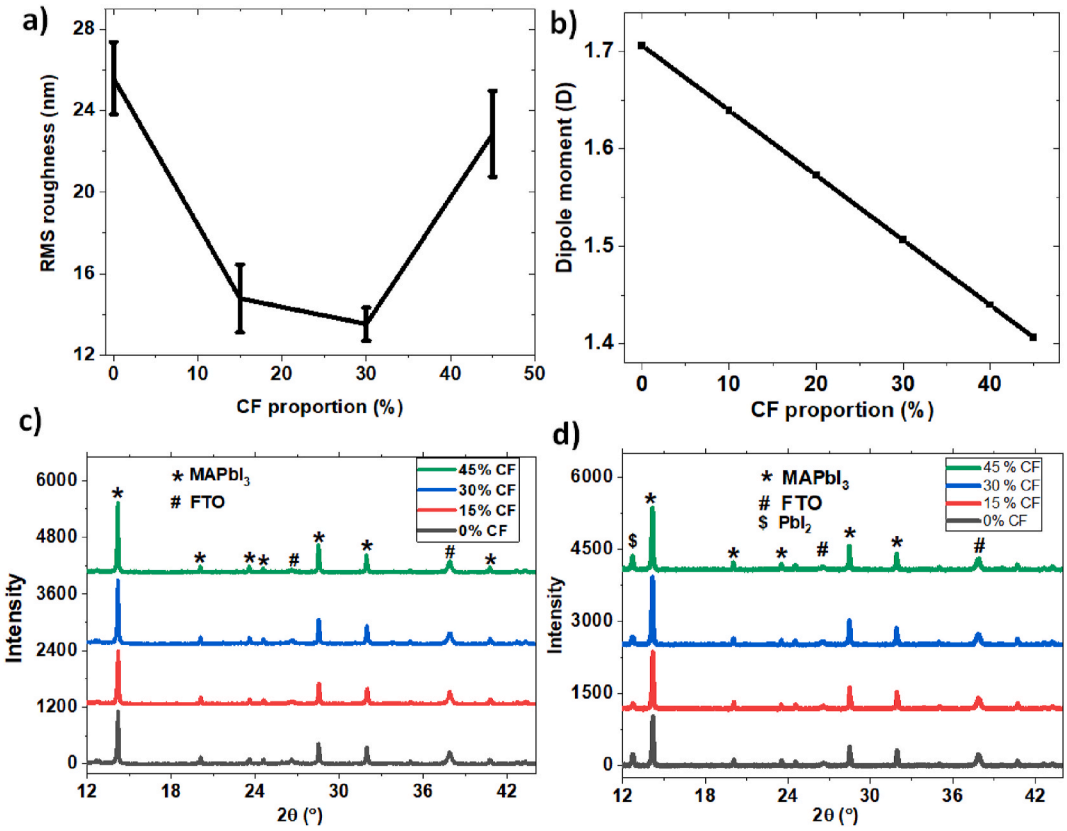

Fig. 5. The effect of chloroform in the mixed antisolvent on (a) RMS roughness of $MAPbI_3$ films (b) Dipole moment of antisolvent (c) XRD spectra of $MAPbI_3$ films at 0 h and (d) XRD spectra of $MAPbI_3$ films after 384 h storage. The films were deposited at 4000 rpm for 30 s and annealed at 110 °C for 15 min under 50–55% RH.

[45]. The peak at 14.02° (110) is the preferred crystal growth direction for the $MAPbI_3$ films while the peak at 37.9° is the preferred crystal direction for the FTO layer. The XRD measurements show that the ratio of the $MAPbI_3$ peak intensity at 14.02° to the FTO peak intensity at 37.9° increases with an increase in the chloroform percentage. Since the peak intensity of $MAPbI_3$ films is strongly affected by the thickness of the films, the observed increase in the peak intensity suggests that an increase in the chloroform percentage of the mixed antisolvent results in an increase in the thickness of $MAPbI_3$ films. It has been reported that the film thickness increases as the amount of $MAPbI_3$/DMSO washed off by the antisolvent was reduced due to an increase in the chloroform percentage [28–30].

In addition, the XRD spectra measured after 384 h (Fig. 5(d)) show that the peak intensity at 14.02° ($MAPbI_3$) relative to the peak intensity at 37.9° (FTO peak) degraded by about 9% for the films treated with the methyl acetate only, while the degradation is 0%, 0% and 15% for the films treated using the mixed antisolvents with 15%, 30% and 45% chloroform, respectively. This result indicates that the thickness of the $MAPbI_3$ films remains unchanged for the films treated using the mixed antisolvents with 15% and 30% chloroform while the thickness of the $MAPbI_3$ films was reduced for the films treated by methyl acetate only or by the mixed antisolvent with 45% chloroform. It can also be seen from Fig. 5(d) that the PbI_2 phase emerges for all devices after 384 h of storage, which is an indication of the decomposition of $MAPbI_3$ due to moisture penetration and protonation [46]. Furthermore, a careful inspection of the peak intensity of the PbI_2 phase reveals that the devices treated using the antisolvent with 15% chloroform produced the least amount of PbI_2 phase after 384 h, indicating better device stability.

The $MAPbI_3$ films were characterised using the UV-VIS technique. Fig. 6(a)–6(d) show the measured absorbance spectra and corresponding Tauc plots at 0 h and after 360 h of storage, respectively. The results show that the absorbance of $MAPbI_3$ films over the wavelength range of 400 nm–500 nm was increased for the films treated using the mixed antisolvent compared to that treated with methyl acetate only. This indicates that the light absorption by the $MAPbI_3$ films was also improved slightly in addition to the improvement in the surface roughness. The UV-VIS measurements after 360 h show that the absorbance of the films treated with the mixed antisolvent remains higher than those treated with only methyl acetate. Comparing the absorbance data obtained at 0 h and after 360 h, the average absorbance of the films treated using only the methyl acetate degraded by about 5%, while it is 0%, 2% and 2% for the films treated with the mixed antisolvent of 15%, 30% and 45% of chloroform, respectively. The films treated with methyl acetate mixed with 15% of chloroform suffered the least degradation as the films have improved grain compactness as indicated by the SEM image in Fig. 3(b). It is anticipated that the improvement in the grain compactness of the $MAPbI_3$ will be beneficial to improving the stability and efficiency of the PSC.

The Tauc plots derived from the measured absorbance show that the energy bandgap (E_g) is about 1.59 eV for all $MAPbI_3$ films investigated, indicating that mixing chloroform with methyl acetate has a negligible effect on the E_g of the $MAPbI_3$ films.

3.2. Photovoltaic performances

Fig. 7(a) presents the current density-voltage (J-V) curves of the best devices treated using the mixed antisolvent of different chloroform percentages. The key electrical parameters for these devices, together with the average values of all devices in a batch are listed in Table 2. The results show that the average J_{sc}, FF and PCE of the devices increase slightly with increasing the chloroform percentage from 0% to 30%. An increase in J_{sc} is due to the improved photon absorption (Fig. 6(a)). An increase in the fill factor (FF) indicates an improved carrier extraction, which is supported by EIS measurement. Fig. 7(b) shows the chemical

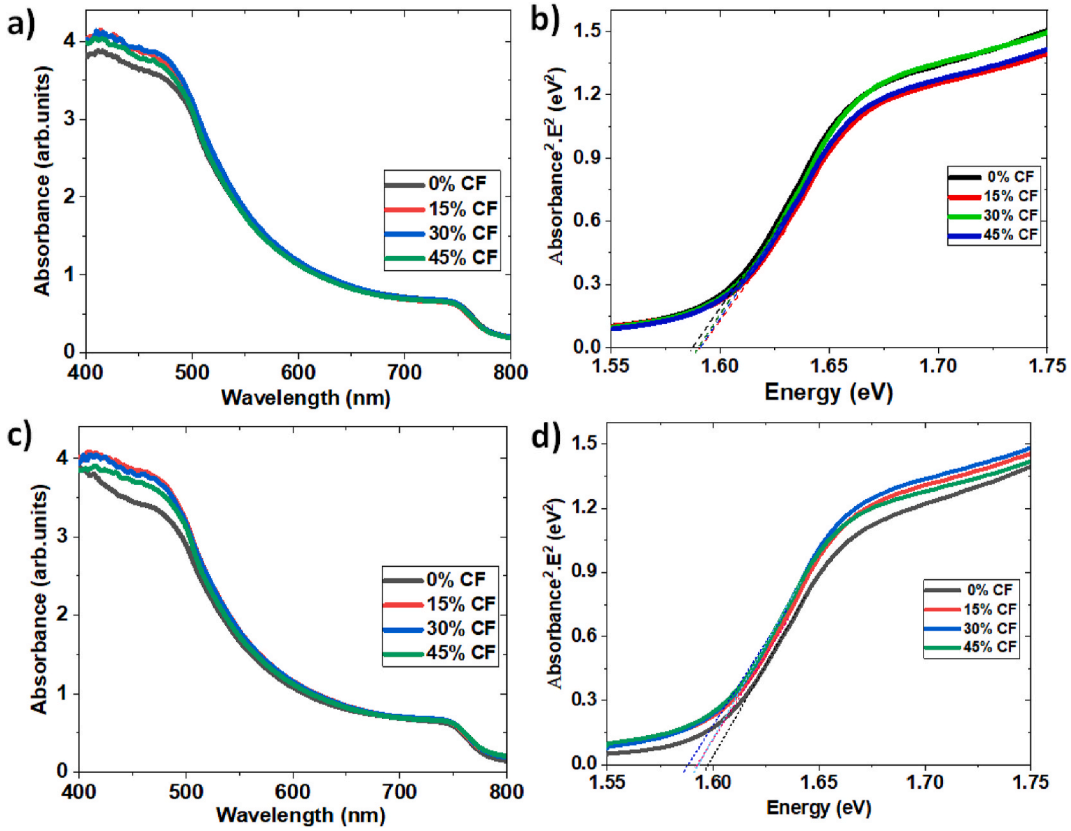

Fig. 6. The optical properties of the $MAPbI_3$ films treated by the mixed antisolvents with different percentages of chloroform (CF). (a) the absorbance of $MAPbI_3$ films after 0 h, (b) Tauc plots of $MAPbI_3$ films after 0 h, (c) absorbance of $MAPbI_3$ films after 360 h, and (d) Tauc plots of $MAPbI_3$ films after 360 h. The films were deposited at 4000 rpm for 30 s and annealed at 110 °C for 15 min under 50–55% RH.

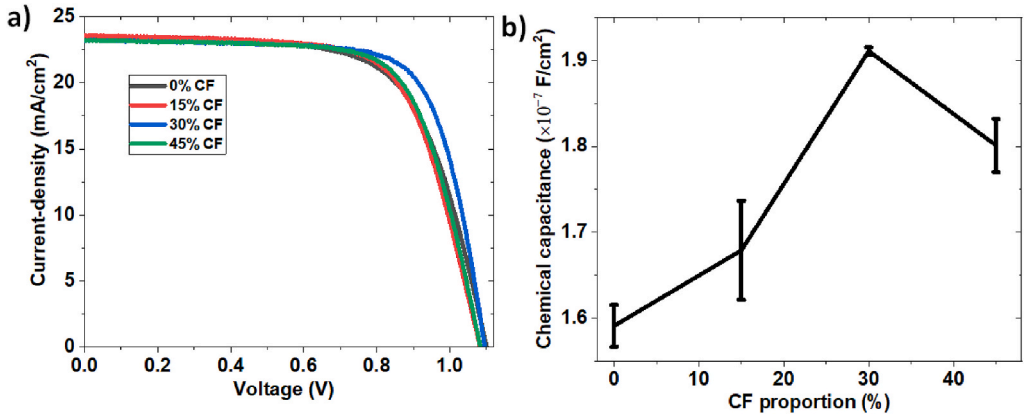

Fig. 7. (a) J-V curves of the devices and (b) Chemical capacitance of the devices as a function of chloroform percentage. The films were deposited at 4000 rpm for 30 s, annealed at 110 °C for 15 min and the devices were fabricated under 50–55% RH.

capacitance as a function of the chloroform percentage of the mixed antisolvent. It has been established that the chemical capacitance derived from EIS measurement is proportional to the carrier density of PSCs [6,47–49]. The results show that the chemical capacitance reaches a peak at 30% of chloroform, indicating that the best charge extraction was obtained using a mixed antisolvent with 30% of chloroform. When the chloroform percentage is increased to 45%, a decrease in the chemical capacitance implies a less effective charge carrier extraction. Consequently, the J_{sc}, FF, and PCE are reduced. Although the devices treated with 15% of chloroform exhibit similar surface smoothness to those treated with 30% of chloroform, their PCE is slightly lower than those treated with 30% of chloroform. This is probably because the devices treated with 30% chloroform have slightly larger grains.

3.3. Device stability

The effect of the mixed antisolvent on the stability of the solar cells was also investigated. The J-V characteristics of the devices were obtained after 0, 216, 360 and 552 h of storage in a desiccator. The V_{oc}, J_{sc}, FF and PCE of the devices were determined from the measured J-V characteristics and the results are shown in Fig. 8(a)–8(d). It can be seen from Fig. 8(a) that the V_{oc} are remarkably similar and remains virtually unchanged after 552 h for all devices treated with different percentages of chloroform. On the other hand, the J_{sc} shows a general trend of

Table 2
Electrical parameters of the perovskite solar cells treated by the mixed methyl acetate-chloroform antisolvent of different chloroform percentages (the rows denoted "Best" represent the data obtained from the best solar cells of the batch; the rows denoted "Av" represent the average of all cells in a batch).

CF Proportion (%)		V_{oc} (V)	J_{sc} (mA/cm^2)	R_s (Ω)	R_p (kΩ)	FF (%)	PCE (%)
0	Best	1.10	23.49	57	13.9	66.08	17.13
	Av.	1.09 ± 0.02	21.99 ± 1.02			64.72 ± 1.37	15.48 ± 0.92
15	Best	1.08	23.62	57	19.5	67.70	17.34
	Av.	1.09 ± 0.02	22.66 ± 1.10			65.92 ± 3.38	16.21 ± 1.15
30	Best	1.10	23.26	42	20.0	72.76	18.55
	Av.	1.09 ± 0.02	22.70 ± 0.93			69.59 ± 2.05	17.16 ± 0.94
45	Best	1.09	23.27	55	13.0	69.66	17.59
	Av.	1.09 ± 0.01	22.33 ± 1.36			68.20 ± 1.77	16.55 ± 1.06

decrease with time for all devices. However, the degradation in the devices treated with the mixed antisolvent is less significant than the degradation in the device treated with the methyl acetate only. The J_{sc} of the devices treated with only methyl acetate degraded by about 10% after 552 h, while they are 3%, 6% and 4% for the devices treated with the mixed antisolvent of 15%, 30% and 45% of chloroform, respectively.

Fig. 8 (c) shows that the fill factor (FF) exhibits the least degradation of 3% for the device treated using the mixed antisolvent with 15% chloroform compared to degradation of 13% for the devices treated with methyl acetate alone. The devices treated using the mixed antisolvents with 30% and 45% chloroform show degradation of 10% and 14%, respectively. Fig. 8(d) shows that the devices treated with methyl acetate only have the worst stability in terms of the PCE, which degraded by about 22%, compared to only 7% for the devices treated using the mixed antisolvent with 15% chloroform after 552 h. The results also show that the PCE of the devices treated using the mixed antisolvent with 30% and 45% of chloroform degraded by 15% and 17%, respectively. These results show clearly that all the devices treated using the mixed antisolvent of different percentages of chloroform show a reasonable degree of stability improvement. Among them, the mixed antisolvent with 15% chloroform exhibits the most significant improvement. The results demonstrate a clear correlation between the stability and surface smoothness and the degradation is associated with the decomposition of $MAPbI_3$ films, which can be mitigated by antisolvent treatment using appropriate mixtures. It is interesting to note that the J_{sc}, FF and PCE of some devices are increased slightly after a period of 150 h of storage before starting to decrease with further increase in storage time. This is likely due to an increase in the conductivity of HTL because of the further oxidation of the Spiro-OMETAD films during storage period [50]. This trend has also been reported in Refs. [13,51,52].

4. Conclusion

A new mixed antisolvent, consisting of methyl acetate and chloroform, was developed for the fabrication of high-quality perovskite films in high humidity (>50%) ambient. The methyl acetate was chosen because of its high-water solubility that facilitates the extraction of DMF in a high humidity environment. The chloroform was chosen because of its relatively low dipole moment that enables adjustment of the dipole

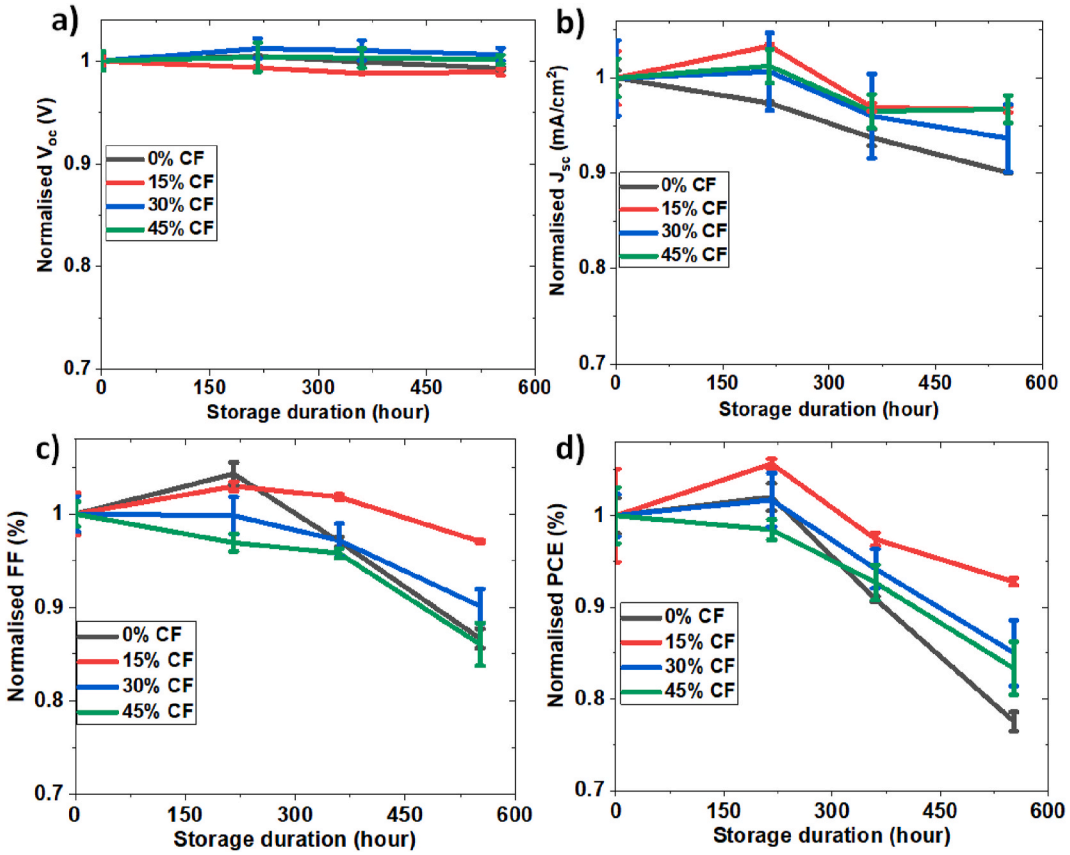

Fig. 8. (a) Open-circuit voltage (V_{oc}), (b) short current density (J_{sc}), (c) fill factor (FF), and (d) power conversion efficiency (PCE) as a function of storage duration for the devices treated with different percentages of chloroform in the mixed antisolvent.

moment of the mixed antisolvent when it is mixed with methyl acetate. The results show that the surface roughness of the perovskite films was significantly improved using a mixed antisolvent of methyl acetate and chloroform with an appropriate percentage. As a result, the efficiency and stability of the perovskite solar cells can be improved for these fabricated in high humidity ambient and treated using this new mixed antisolvent. The devices treated with methyl acetate mixed with 30% chloroform exhibit the best PCE of 18.55% compared to 17.13% for the devices treated with methyl acetate only. In addition, slow degradation of only 7% in the PCE after 552 h of storage was observed in the devices treated with the methyl acetate mixed with 15% chloroform, compared to 22% for the devices treated with methyl acetate only. Although the best improvement for the efficiency and stability corresponds to different percentages of chloroform addition, both the efficiency and stability are increased compared to the films treated with only one antisolvent. These results demonstrate the usefulness and benefits of this new mixed antisolvent for the fabrication of high-quality perovskite films in high humidity ambient. Compared to the methods of employing an additional passivation layer, this mixed antisolvent process provides a simple and low-cost manufacturing route towards the improvement of both stability and efficiency.

Declaration of competing interest

The authors declare that they have no known competing financial interests or personal relationships that could have appeared to influence the work reported in this paper.

Acknowledgement

Martin Eze wishes to thank the Federal Government of Nigeria for the financial support of his PhD study under the Petroleum Technology Development Fund PTDF/ED/PHD/EMC/1091/17. A special thanks go to Mr J Rowland for assistance in XRD and UV–Visible spectroscopy. Dr Daniel Zabek is thanked for his assistance in SEM measurement. EPSRC is acknowledged for partial support of facilities for the fabrication and characterisation of solar cells under the projects EP/K029142/1, and EPK022156/1.

References

[1] S. Wang, et al., Titanium-defected undoped anatase TiO2with p-type conductivity, room-temperature ferromagnetism, and remarkable photocatalytic performance, J. Am. Chem. Soc. 137 (2015) 2975–2983.
[2] N. Zhang, et al., Highly reproducible organometallic halide perovskite microdevices based on top-down lithography, Adv. Mater. 29 (2017) 9–10.
[3] G.E. Eperon, et al., Formamidinium lead trihalide: a broadly tunable perovskite for efficient planar heterojunction solar cells, Energy Environ. Sci. 7 (2014) 982.
[4] D. Li, F. Sun, C. Liang, Z. He, Effective approach for reducing the migration of ions and improving the stability of organic-inorganic perovskite solar cells, J. Alloys Compd. 741 (2018) 489–494.
[5] M. Alidaei, M. Izadifard, M.E. Ghazi, V. Ahmadi, Efficiency enhancement of perovskite solar cells using structural and morphological improvement of CH3NH3PbI3 absorber layers, Mater. Res. Express 5 (2018).
[6] Eze, et al., Optimum silver contact sputtering parameters for efficient perovskite solar cell fabrication, Sol. Energy Mater. Sol. Cell. 230 (2021), 111185.
[7] A. Kojima, K. Teshima, Y. Shirai, T. Miyasaka, Organometal halide perovskites as visible-light sensitizers for photovoltaic cells, J. Am. Chem. Soc. 131 (2009) 6050–6051.
[8] M. Jeong, et al., Stable perovskite solar cells with efficiency exceeding 24.8% and 0.3-V voltage loss, Science 369 (2020) 1615–1620.
[9] J.J. Yoo, et al., Efficient perovskite solar cells via improved carrier management, Nature 590 (2021) 587–593.
[10] B. Conings, et al., Intrinsic thermal instability of methylammonium lead trihalide perovskite, Adv. Energy Mater. 5 (2015) 1–8.
[11] Q. Tai, et al., Efficient and stable perovskite solar cells prepared in ambient air irrespective of the humidity, Nat. Commun. 7 (2016) 1–8.
[12] Q. Wang, et al., Stabilizing the α-phase of CsPbI3Perovskite by sulfobetaine zwitterions in one-step spin-coating films, Joule 1 (2017) 371–382.
[13] C. Yi, et al., Entropic stabilization of mixed A-cation ABX 3 metal halide perovskites for high performance perovskite solar cells, Energy Environ. Sci. 9 (2016) 656–662.
[14] X. Qin, et al., Recent progress in stability of perovskite solar cells, J. Semiconduct. 38 (2017) 1–8.
[15] C.C. Stoumpos, C.D. Malliakas, M.G. Kanatzidis, Semiconducting tin and lead iodide perovskites with organic cations: phase transitions, high mobilities, and near-infrared photoluminescent properties, Inorg. Chem. 52 (2013) 9019–9038.
[16] F. Gao, et al., Enhanced performance of tin halide perovskite solar cell by addition of lead thiocyanate, RSC Adv. 8 (2018) 14025–14030.
[17] J. Xiang, K. Wang, B. Xiang, X. Cui, Sn 2+ —stabilization in MASnI 3 perovskites by superhalide incorporation, J. Chem. Phys. 148 (2018), 124111.
[18] C. Ran, et al., Bilateral interface engineering toward efficient 2D-3D bulk heterojunction tin halide lead-free perovskite solar cells, ACS Energy Lett. 3 (2018) 713–721.
[19] Q. Fu, et al., Recent progress on the long-term stability of perovskite solar cells, Adv. Sci. 5 (2018).
[20] Y. Wang, et al., Largely enhanced V_{OC} and stability in perovskite solar cells with modified energy match by coupled 2D interlayers, J. Mater. Chem. 6 (2018) 4860–4867.
[21] F. Yang, et al., Dependence of acetate-based antisolvents for high humidity fabrication of CH3NH3PbI3Perovskite devices in ambient atmosphere, ACS Appl. Mater. Interfaces 10 (2018) 16482–16489.
[22] J. Troughton, K. Hooper, T.M. Watson, Humidity resistant fabrication of CH3NH3PbI3perovskite solar cells and modules, Nano Energy 39 (2017) 60–68.
[23] J. Chen, J. Ren, Z. Li, H. Wang, Y. Hao, Mixed antisolvents assisted treatment of perovskite for photovoltaic device efficiency enhancement, Org. Electron.: physics, materials, applications 56 (2018) 59–67.
[24] Y. Tu, et al., Controlled growth of CH3NH3PbI3films towards efficient perovskite solar cells by varied-stoichiometric intermediate adduct, Appl. Surf. Sci. 403 (2017) 572–577.
[25] Y. Rahaq, M. Moussa, A. Mohammad, H. Wang, A. Hassan, Highly reproducible perovskite solar cells via controlling the morphologies of the perovskite thin films by the solution-processed two-step method, J. Mater. Sci. Mater. Electron. 29 (2018) 16426–16436.
[26] Y. Chen, W. Wu, R. Ma, C. Wang, Perovskites fabricated with volatile anti-solvents for more efficient solar cells, J. Mol. Struct. 1175 (2018) 632–637.
[27] Z. Huang, D. Wang, S. Wang, T. Zhang, Highly efficient and stable $MAPbI_3$perovskite solar cell induced by regulated nucleation and ostwald recrystallization, Materials 11 (2018) 20–30.
[28] M. Xiao, et al., Selection of an anti-solvent for efficient and stable cesium-containing triple cation planar perovskite solar cells, Nanoscale 10 (2018) 12141–12148.
[29] A.D. Taylor, et al., A general approach to high-efficiency perovskite solar cells by any antisolvent, Nat. Commun. 12 (2021) 1–11.
[30] L. Wang, et al., The mechanism of universal green antisolvents for intermediate phase controlled high-efficiency formamidinium-based perovskite solar cells, Mater. Horiz. 7 (2020) 934–942.
[31] NIOSH Pocket Guide to Chemical Hazards. DHHS (NIOSH) Publication 2005-149, (2007).
[32] Solvent Miscibility Table. Available at: https://www.sigmaaldrich.com/chemistry/solvents/solvent-miscibility-table.html. (Accessed: 29th November 2020).
[33] Y. Wang, et al., Stitching triple cation perovskite by a mixed anti-solvent process for high performance perovskite solar cells, Nano Energy 39 (2017) 616–625.
[34] K.M. Lee, et al., Effect of anti-solvent mixture on the performance of perovskite solar cells and suppression hysteresis behavior, Org. Electron. 65 (2019) 266–274.
[35] J. Yi, et al., Regulated perovskite crystallinity via green mixed antisolvent for efficient perovskite solar cells, Org. Electron. 69 (2019) 69–76.
[36] Y. Wang, et al., Stitching triple cation perovskite by a mixed anti-solvent process for high performance perovskite solar cells, Nano Energy 39 (2017) 616–625.
[37] Y. Yu, et al., Ultrasmooth perovskite film via mixed anti-solvent strategy with improved efficiency, ACS Appl. Mater. Interfaces 9 (2017) 3667–3676.
[38] K. Jung, et al., Ambient-air fabrication of stable mixed cation perovskite planar solar cells with efficiencies exceeding 22% using a synergistic mixed antisolvent with complementary properties, Nano Energy 89 (2021), 106387.
[39] N. Ahn, et al., Highly reproducible perovskite solar cells with average efficiency of 18.3% and best efficiency of 19.7% fabricated via lewis base adduct of lead(II) iodide, J. Am. Chem. Soc. 137 (2015) 8696–8699.
[40] H. Liu, et al., π-Conjugated small molecules enable efficient perovskite growth and charge-extraction for high-performance photovoltaic devices, J. Power Sources 448 (2020), 227420.
[41] H.A. Rizk, I.M. Elanwar, Dipole moments of glycerol, isopropyl alcohol, and isobutyl alcohol, Can. J. Chem. 46 (1968) 507–513.
[42] A.V. Gubskaya, P.G. Kusalik, The total molecular dipole moment for liquid water, J. Chem. Phys. 117 (2002) 5290–5302.
[43] T. Vasiltsova, A. Heintz, New statistical mechanical model for calculating Kirkwood factors in self-associating liquid systems and its application to alkanol+ cyclohexane mixtures, J. Chem. Phys. 127 (2007).
[44] J.C.R. Reis, T.P. Iglesias, Kirkwood correlation factors in liquid mixtures from an extended Onsager-Kirkwood-Fröhlich equation, Phys. Chem. Chem. Phys. 13 (2011) 10670–10680.
[45] Q. Sun, et al., Efficiency enhancement of perovskite solar cells via electrospun CuO nanowires as buffer layers, *ACS Applied Materials & Interfaces* acsami (2018), 7b19335, https://doi.org/10.1021/acsami.7b19335.
[46] C.C. Boyd, R. Cheacharoen, T. Leijtens, M.D. McGehee, Understanding degradation mechanisms and improving stability of perovskite photovoltaics, Chem. Rev. 119 (2019) 3418–3451.

[47] I. Mora-Seró, G. Garcia-Belmonte, P.P. Boix, M.A. Vázquez, J. Bisquert, Impedance spectroscopy characterisation of highly efficient silicon solar cells under different light illumination intensities, Energy Environ. Sci. 2 (2009) 678–686.
[48] J. Bisquert, Chemical capacitance of nanostructured semiconductors: its origin and significance for nanocomposite solar cells, Phys. Chem. Chem. Phys. 5 (2003) 5360–5364.
[49] J. Bisquert, L. Bertoluzzi, I. Mora-Sero, G. Garcia-Belmonte, Theory of impedance and capacitance spectroscopy of solar cells with dielectric relaxation, drift-diffusion transport, and recombination, J. Phys. Chem. C 118 (2014) 18983–18991.
[50] Y. Wang, H. Qu, C. Zhang, Q. Chen, Rapid oxidation of the hole transport layer in perovskite solar cells by A low-temperature plasma, Sci. Rep. 9 (2019) 1–9.
[51] Z. Li, et al., Stabilizing perovskite structures by tuning tolerance factor: formation of formamidinium and cesium lead iodide solid-state alloys, Chem. Mater. 28 (2016) 284–292.
[52] G.W. Kim, G. Kang, M. Malekshahi Byranvand, G.Y. Lee, T. Park, Gradated mixed hole transport layer in a perovskite solar cell: improving moisture stability and efficiency, ACS Appl. Mater. Interfaces 9 (2017) 27720–27726.